The optical calibration of the BigBite spectrometer with the Hadron detector package in Hall A at Jefferson Lab

Abstract

Keywords: Jefferson Lab, Hall A, Instrumentation, E05-102, BigBite, Optical calibration

1. Introduction

One of the recent acquisitions in the experimental Hall A of the Thomas Jefferson National Accelerator Facility (TJNAF) is the BigBite spectrometer. This device was previously used at the NIKHEF facility as the electron spectrometer [1, 2]. At Jefferson Lab, BigBite has recently been re-implemented as a versatile large-acceptance spectrometer that could be outfitted with various detector packages depending on the particular requirements of the experiments. The spectrometer is an addition to the High-Resolution Spectrometers (HRS-L and HRS-R) that are the standard equipment of Hall A [3], allowing for more flexible experimental setups involving double- and even triple-coincidence measurements.

BigBite has been used in two large groups of experiments that were performed in 2008 and 2009, and were dealing with a broad range of physics topics. Among others, we studied neutral pion production on protons close to threshold (experiment E04-007 [4]); measured single-spin asymmetries in semi-inclusive pion electro-production on polarized ^{3}He (experiments E06-010 and E06-011 [5, 6]); determined the parallel and perpendicular asymmetries on polarized ^{3}He in order to extract the $g_2^{\rm n}$ structure function in the deep-inelastic regime (experiment E06-014 [7]); and measured the double-polarization asymmetries A'_x and A'_z in the quasi-elastic processes He(e, e′d), He(e, e′p), and He(e, e′n) (experiment E05-102 [8]). This paper describes the optical calibration of the BigBite spectrometer with the detector package configured for the detection of hadrons, as it has been used in the E05-102 experiment.

2. Experimental details

Experiment E05-102 was performed in Hall-A [3] at Thomas Jefferson National Accelerator Facility. In the experiment a polarized ^{3}He target was used in conjuction with a polarized continuum electron beam. Scattered electrons ware detected with the High Resolution Spectrometer (HRS-L) in coincidence with protons and deuterons detected by the large-acceptance spectrometer BigBite. Beside the helium target, carbon target and gasous hydrogen and deuterium targets were used for calibration. Various kinematical settings were considered, with momentum-transfer vector $\vec{q}$ pointing in the direction of BigBite. This way elastic and quasi-elastic protons and deuterons were within the BigBite acceptance. For a 1.245 GeV running, HRS-L was positioned at 17° and BigBite at $-74°$ with respect to the direction of the incomming electron beam. Afterwards, BigBite was moved to $-75°$ for the experiments with 2.425 GeV and 3.606 GeV electrons. HRS-L was then at 14.5° and at 12.5°.

3. BigBite Spectrometer

BigBite is a non-focusing spectrometer with large momentum and angular acceptance [1]. It consists of a single normal-conducting clam-shell dipole magnet. For a mean field density of 0.92 T, a 518 A current is used. This corresponds to a central momentum of 500 MeV/c and bending angle of 25 deg. The magnet is followed by the hadron detector package, which consists of two Multi-Wire-Drift-Chambers (MWDC) for tracking and two planes of scintillation detectors for triggering, particle identification and energy determination. Each MWDC consists of six wire-planes. Wires in first two planes are positioned horizontaly, while the wires in the third and fourth plane are oriented at angle 30 deg with respect to the horizontal line. Wires of the last two planes are oriented at -30 deg. Wire-planes in first MWDC contain 141 wires. Second MWDC is bigger and consists of 200 wires per wire-plane. Wires in both planes are 1 cm apart. Trigger planes dE and E are built of 24 bars, made of EJ-204 plastic scintillator. Each bar is 50 cm long and 8.6 cm wide. For the dE-plane thin, 0.3 cm, bars were used, to detect low energy particles, while for E-plane thicker 3 cm bars were considered for detection of more energetic particles. Signal from each bar is detected with two XP2262 photomultiplier tubes,

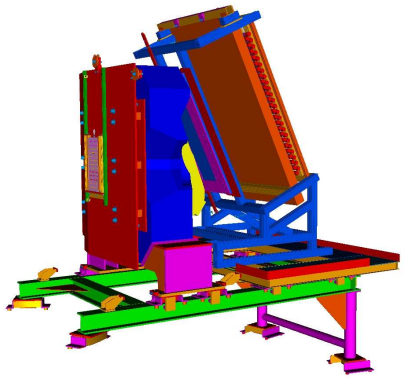

Figure 1: BigBite Spectrometer with the hadron detector package mounted on a supprot frame

mounted on both ends of a bar. To double spacial and momentum resolution, E-plane is shifted for half of a paddle with respect to the dE-plane.

4. Optical calibration

The purpose of optical calibration is to determine target variables, that have physical meaning from the detector variables, that are measured directly. In BigBite two position coordinates x_{Det} and y_{Det} and two angles θ_{Det} and ϕ_{Det} are measured. From this information vertex position y_{Tg}, in-plane and out-of-plane scattering angles, ϕ_{Tg} and θ_{Tg}, and a relative particle momentum δ_{Tg} are reconstructed. This can be done in many ways. For BigBite analytical model was considered, followed by more sophisticated transport-matrix-formalism approach.

4.1. Analytical model

Analytical model served as a starting point for BigBite optics. Due its simplicity it could be quickly implemented, tested and used on experimental data to get first estimation of the experimental results. In BigBite magnet field is oriented in y_{Tg} direction (see Fig. 2). According to [1], BigBite has almost constant field-density inside the magnet, accompanied by fringe-fields on the edges, which are falling exponentially, when moving away from the magnet. In the analytical model, true field was approximated by a constant magnetic field within the effective field boundaries and neglecting any edge effects.

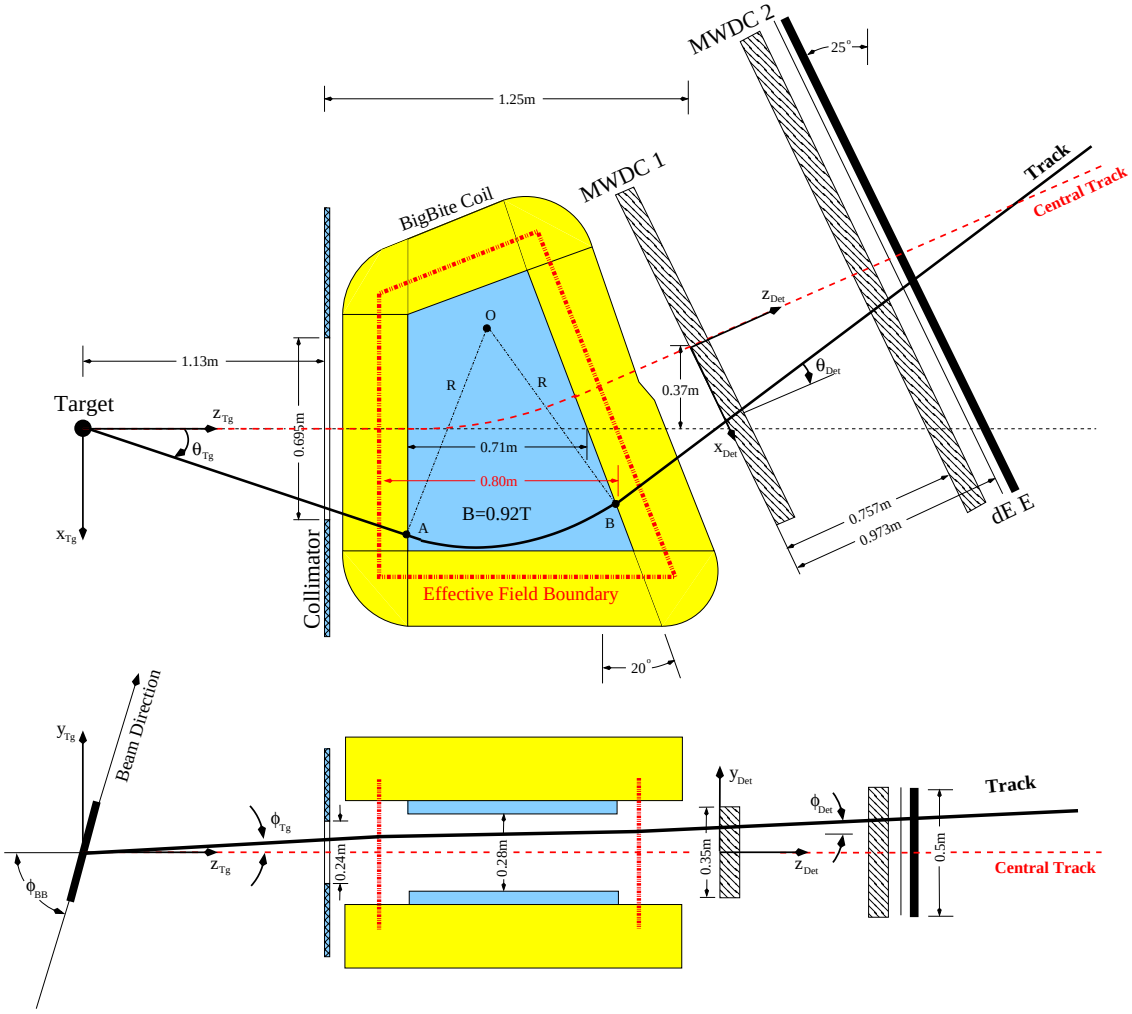

Figure 2: View of the dispersive and non-dispersive plane of BigBite spectrometer. A small angular deflection in a non-dispersive plane occours if trajectory is not perpendicular to the effective-field boundary [2]. This correction was calculated by Penner [**?**] and was estimated to be (≈ 18 mrad). Since opposite effects happen at the entrance and exit field boundary, non-dispersive angle remains unchanged.

This way a circular-arc model could be applied for the determination of all target coordinates. The description of particle transport inside the magnet can be divided into a free particle motion in the $y - z$ plane and a circular motion in $x - z$ plane, which is

described by the Lorentz equation

$$p_y = \text{const.}\,, \quad p_{xz} = eRB_y \tag{1}$$

To determine momentum, first radius of the trajectory needs to be calculated. This can be done using the track information in the detector package together with geometrical properties of BigBite spectrometer, by satisfying conditions

$$\overline{ATg} \perp \overline{AO},\ \overline{OB} \perp \overline{BD},\ |\overline{AO}| = |\overline{BO}| = R \tag{2}$$

This dictates relations between points A, B, O, Tg, D written in the target coordinate system:

$$x_O = -\frac{z_{Tg}}{x_A}(z_O - z_A) + x_A = -\frac{z_D - z_B}{x_D - x_B}(z_O - z_B) + x_B \tag{3}$$

$$R^2 = (z_O - z_A)^2 \left[1 + \left(\frac{z_{Tg}}{z_A}\right)^2\right] = (z_B - z_O)^2 \left[1 + \left(\frac{z_D - z_B}{x_D - x_B}\right)^2\right] \tag{4}$$

Point B where particle exits the magnet is the intersection between an extrapolation of the particle track in the detector-package and a effective exit-face of the magnet and can be easily calculated. Component z_A of point A corresponds to a known distance between the target and effective entrance to the BigBite magnet. By expressing z_O from (3) and inserting it into (4), an equation for x_A is obtained. In general this equation has three complex solutions. The correct result for x_A should analyticaly be a real number and should lie within the effective field boundaries. Two additional physical constraints are applied. Particle track should always represent a shorter arc of the circle and it should move counter clockwise with respect to O if the magnetic field is pointing in direction of y_{Tg}, or clockwise if the magnetic field is pointing in the opposite direction. Once knowing the correct solution, radius R can be determined, together with a momentum p_{xz}. A particle flight path l_{xz} in the x-z plane, can also be calculated using the cosine formula for angle $\beta = \measuredangle AOB$

$$\begin{aligned} l_{xz} &= \sqrt{z_A^2 + x_A^2} + R\beta + \sqrt{(z_D - z_B)^2 + (x_D - x_B)^2}\,, \\ \cos\beta &= \frac{(z_A - z_O)(z_B - z_O) + (x_A - x_O)(x_B - x_O)}{R^2}\,. \end{aligned} \tag{5}$$

Using this information, all target coordinates can be directly expressed as

$$\phi_{\text{Tg}} = \phi_{\text{Det}}$$

$$
\begin{aligned}
\theta_{\mathrm{Tg}} &= \frac{x_A}{z_A} \\
y_{\mathrm{Tg}} &= y_{\mathrm{Det}} - l_{xz}\phi_{\mathrm{Det}} \\
\delta_{\mathrm{Tg}} &= \frac{p_{xz}}{p_c}\frac{\sqrt{1+\phi_{\mathrm{Tg}}^2+\theta_{\mathrm{Tg}}^2}}{\sqrt{1+\theta_{\mathrm{Tg}}^2}} \\
L &= l_{xz}\sqrt{1+\phi_{\mathrm{Tg}}^2}
\end{aligned}
\tag{6}
$$

where p_c is a central momentum of BigBite spectrometer. With the presented analytical approximation of BigBite optics, resolution up to few percent can be achieved, but decreases when away from the center of BigBite acceptance, especially for ϕ_{Tg}. There, fringe-fields start to affect the optics. As shown, model requires only few geometrical parameters, but they need to be well known in order for model to work. Distances between different parts of spectrometer and sizes could be in principal determined from the calibration with elastic events. However, the solution is not unique. Different combinations of geometrical parameters could give almost identical results for BigBite target variables, but only one combination is correct. Therefore without a good information about geometrical properties of BigBite, analytical model will not work properly.

4.2. The matrix formalism

With this approach a prescription is obtained, that transforms detector variables directly to the target variables. Various parameterizations are possible. For BigBite a polynomial expansion of form

$$
\Omega_{\mathrm{Tg}} = \sum_{i,j,k} \theta_{\mathrm{Det}}^i y_{\mathrm{Det}}^j \phi_{\mathrm{Det}}^k \sum_{l=0}^{7} a_{ijkl}^{\Omega_{\mathrm{Tg}}} x_{det}^l \,, \qquad \Omega_{\mathrm{Tg}} \in \{\delta_{\mathrm{Tg}}, \theta_{\mathrm{Tg}}, \phi_{\mathrm{Tg}}, y_{\mathrm{Tg}}\} \,, \tag{7}
$$

has been considered. Although the form is polynomial, can this expansion be interpreted in terms of vector algebra as a scalar product of vector $\{x_{\mathrm{Det}}^l\}$ with the vector $\{\theta_{\mathrm{Det}}^i y_{\mathrm{Det}}^j \phi_{\mathrm{Det}}^k\}$ and a tensor-like form $a_{ijkl}^{\Omega_{\mathrm{Tg}}}$, were all expansion parameters are gathered. This notation was used in our procedure and is called a transport-matrix formalism. Knowing the optics of the spectrometer means knowing the parameters a_{ijkl} and being aware of the limits where such a parameterization works. The polynomial expansion is easy to handle, but one must precisely understand the contribution of the high-degree terms. Uncontrolled inclusion of these terms can cause oscillations of the reconstructed

variables, especially on the edges of the acceptance. A main goal is therefore to find a well behaved low-order optical matrix that has as few high-degree terms as possible.

4.2.1. Direct comparison of detector variables with target coordinates

The determination of the optical matrix started with the low-order analysis in order to get an approximate values for first few matrix elements. As in the analytical model, BigBite magnet was assumed to be an ideal dipole. Therefore in-plane and out-of-plane variables could be decoupled, resulting in $\delta_{\rm Tg}$, $\theta_{\rm Tg}$ depending only on $x_{\rm Det}$, $\theta_{\rm Det}$, while $y_{\rm Tg}$, $\phi_{\rm Tg}$ depending only on $y_{\rm Det}$, $\phi_{\rm Det}$. Since each target coordinate depends only on two detector variables, the matrix elements can be estimated via examination of 2D histograms, showing the direct comparison of target coorinates, determined from HRS-L data, to BigBite detector variables, using various detector-variable cuts. Since BigBite in this approximation does not bend particles in horizontal direction, first-order polynomials were considered to fit data for $y_{\rm Tg}$ and $\phi_{\rm Tg}$, while up to third-order polynomial expansions were applied for $\delta_{\rm Tg}$ and $\theta_{\rm Tg}$:

$$\begin{aligned}
\delta_{Tg}(x,\theta) &= \left[a^{\delta}_{0000} + a^{\delta}_{1000}x + a^{\delta}_{2000}x^2\right] + \left[a^{\delta}_{0100} + a^{\delta}_{1100}x + a^{\delta}_{2100}x^2\right]\theta \\
&+ \left[a^{\delta}_{0200} + a^{\delta}_{1200}x\right]\theta^2 + \left[a^{\delta}_{0300} + a^{\delta}_{1300}x\right]\theta^3 \qquad (8)\\
\theta_{Tg}(x,\theta) &= \left[a^{\theta}_{0000} + a^{\theta}_{1000}x + a^{\theta}_{2000}x^2\right] + \left[a^{\theta}_{0100} + a^{\theta}_{1100}x + a^{\theta}_{2100}x^2\right]\theta \qquad (9)\\
\phi_{Tg}(y,\phi) &= a^{\phi}_{0000} + a^{\phi}_{0001}\phi \qquad (10)\\
y_{Tg}(y,\phi) &= \left[a^{y}_{0001} + a^{y}_{0011}y\right]\phi + \left[a^{y}_{0000} + a^{y}_{0010}y\right] \qquad (11)
\end{aligned}$$

Determined matrix elements are shown in column 2 of table 1. Analysis showed that this approximation could not be used for further physics analysis, because higher order corrections are necessary for representative results. However, low-order terms are very robust, and would not change much when more sophisticated models with higher-degree terms are considered. Therefore results obtained with this method could serve for testing later, more advanced methods. In particular, to check, if calculated matrix elements, obtained with automated numerical algorithms converge to reasnable values.

4.2.2. Numerical Methods

For the determination of BigBite optics matrix, when it is used with hadron detector package, a special numerical method was developed, which consideres up to fourth order

Matrix element	Direct comparison	N & M	SVD	Simul.
$a_{0010}^{y_{Tg}}$	0.998013	1.029	1.00155	1.0765
$a_{0001}^{y_{Tg}}$	-2.80084	-2.8183	-2.7648	-3.113
$a_{0001}^{\phi_{Tg}}$	$1.0^{\dagger}$	1.03678	1.0536	1.2291
$a_{1000}^{\theta_{Tg}}$	0.49681	0.5492	0.5463	0.768
$a_{0100}^{\theta_{Tg}}$	-0.49109	-0.4896	-0.4819	-1.2317
$a_{1000}^{\delta_{Tg}}$	-0.754484	-0.71600	-0.67627	1.7961
$a_{0100}^{\delta_{Tg}}$	2.81136	2.88118	2.80163	5.1449

† $a_{0001}^{\phi_{Tg}}$ was a priori set to 1 in this approximation.

Table 1: Most important BigBite matrix-elements determined with different methods.

matrix elements. Their values are calculated using χ^2-minimization, where calculated target variables (7) are compared with the directly measured values

$$\chi^2\left(a_i^{\Omega_{Tg}}\right) = \sqrt{\left(\Omega_{\mathrm{Tg}}^{\mathrm{Measured}} - \Omega_{\mathrm{Tg}}^{\mathrm{Optics}}\left(x_{det}, y_{det}, \theta_{det}, \phi_{det}; a_i^{\Omega_T g}\right)\right)^2}, \quad i = 1, 2, \ldots, M\,. \tag{12}$$

The use of M matrix elements for each target variable means that a global minimum in a M-dimensional space must be found. Numerically this is a very complex problem. For solving this problem two techniques were considered.

The Downhill Simplex Method developed by Nedler and Mead [9] was our first choice. Method tries to minimize a scalar-valued non-linear function of N parameters. For that it uses only function evaluations and requires no derivative information. It is very easy to use, thus very popular in engineering and science application for non-linear unconstrained optimization. However, this method is not very time efficient and its convergence properties are not well understood, especially when used for minimization in more than two dimension. It is possible that the minimization method will stop in one of the possible local minima instead of the global minimum [11, 12]. Therefore the robustness of the method needed to be examined.

As an alternative to simplex minimization, Singular-Value-Decomposition was considered. Function Ω_{Tg} is a linear function of parameters $a_i^{\Omega_{Tg}}$. This means that (12) can

be written as

$$\chi^2 = \sqrt{|\mathbf{A}\cdot\mathbf{a}-\mathbf{b}|^2}\,, \tag{13}$$

where vector $\mathbf{a}$ contains all M matrix elements and vector $\mathbf{b}$ contains N measured values of considered target variable. Matrix $\mathbf{A}$ of size $N \times M$ is filled with various products of detector variables $a_i^{\Omega_{Tg}}$ for every measured event used for the calibration. Vector $\mathbf{a}$ that minimizes (13) is determined using the SVD method [9**?**]. It is a powerfull tool, which is based on a theorem of linear algebra, that any $N \times M$ matrix, where number of rows N is greater or equal to number of columns M, can be written as a product of an $N \times M$ column-orthogonal matrix $\mathbf{U}$, an $M \times M$ diagonal matrix $\mathbf{W}$ filled with positively definite singular values w_i, and a transpose of an $M \times M$ orthogonal matrix $\mathbf{V}$. In the case of overdetermined system ($N > M$), presented in (13), it produces the best solution in the least-square sense. Therefore no additional robustness tests are required as in previous method. Another great adventage is, that it cannot fail [9]. Method always returns a solution, but its quality depends on quality of the input data. The solution has the form

$$\mathbf{a} = \sum_{i=1}^{M} \left(\frac{\mathbf{U}_i \cdot \mathbf{b}}{w_i} \right) \mathbf{V_i}\,, \tag{14}$$

4.2.3. Calibration data

During experiment various dedicated calibration measurements were made, to be used together with developed numerical methods for the determination of the optics matrix. y_{Tg} was calibrated using quasi-elastic carbon data made with an extensive, 40 cm long, carbon optics-target. It consists of seven thin carbon foils, that are mounted to a plastic frame (see Fig. 4). In addition, a slanted BeO foil is added in front of a target (as a 8th foil) which serves for the visual inspection of the position of the electron beam. For the calibration of θ_{Tg} and ϕ_{Tg}, special set of carbon and deuterium data was considered, where sieve-slit was put in front of a BigBite magnet. The sieve-slit collimator consists of 81 holes that are uniformly positioned over the whole angular acceptance of the spectrometer. The sieve-slit also contains four larger holes for proper horizontal and vertical orientation of the sieve and easier identification of the hole projections at the detector package. In addition, hydrogen elastic data were used for the absolute positioning of the sieve with respect to the optical axis of the BigBite, which can not be determined directly

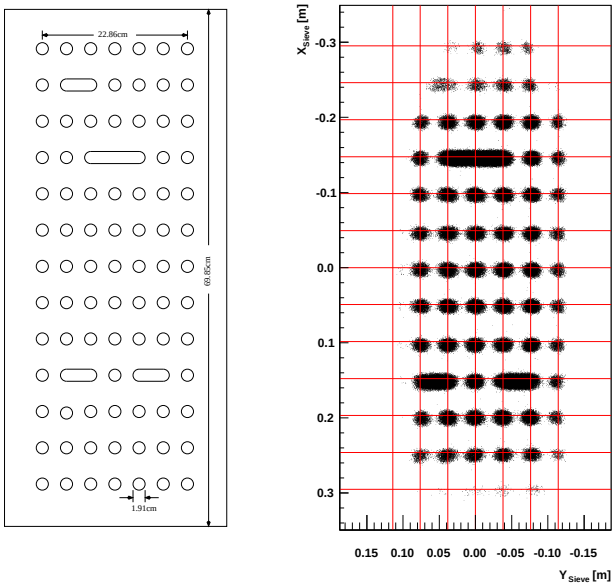

Figure 3: [Left] Schematics of BigBite Sieve-slit collimator, [Right] Reconstructed sieve pattern. Most left holes are missing due to the geometrical obtacles inbetween target and BigBite.

from the quasi-elastic carbon data. The determination of the matrix elements for the δ_{Tg} was done with the hydrogen and deuterium elastic data, where particle momentum in BigBite equals q-vector, determined by the HRS-L.

Various cuts were applied to the collected calibration data to eliminate the noise that could influence the minimization process. Only coincidence events were consided, since various information from HRS-L, such as target coordinates, trigger information and detector variables, were required to calibrate BigBite. This was done via raw coincidence time cut. For additional noise reduction, HRS-L acceptance cuts were applied. Finally, in the calibration only those events were considered, that leave consistent hits in all BigBite detectors and could be consequently joined in a single particle track inside the detector package.

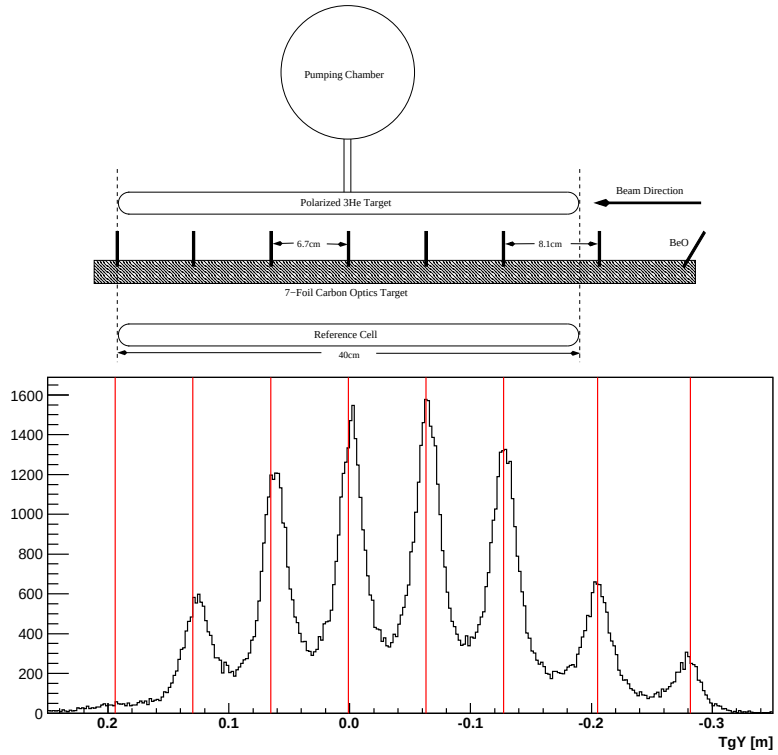

Figure 4: [Up] Target ladder diagram with polarized ^{3}He cell on top, 7-foil carbon optics target in between and gasous reference cell in the bottom. Slanted BeO window was used for visual inspection of beam position. [Down] Reconstructed vertex position $y_{\rm Tg}$ for the 7-foil carbon-optics target, using the SVD technique. Red lines show the exact positions of carbon foils.

4.2.4. Vertex position

The matrix for the vertex position variable $y_{\rm Tg}$ was obtained using 7-foil carbon target. The positions of carbon foils were precisely determined before the experiment. For that a special geodetic survey was used with accuracy ($\leq 100\,\mu$m). This enables a precise $y_{\rm Tg}$ calibration. Which foil did particles detected in BigBite came from, was determined from HRS-L vertex information. This way can detector variables for each coincidence event be directly correlated to the particle position at the target. When (7) is written out for $y_{\rm Tg}$, a linear equation for each event can be formed

$$\begin{aligned} y_{Tg_{(n)}}^{\rm Measured} &= y_{{\rm Tg}_{(n)}}^{\rm Optics} \\ &= a^y_{0000} + a^y_{0001}\phi_{(n)} + a^y_{0002}\phi^2_{(n)} + a^y_{0003}\phi^3_{(n)} + \cdots \end{aligned}$$

$$
\begin{aligned}
&+ \quad a^y_{0010} y_{(n)} + a^y_{0020} y^2_{(n)} + a^y_{0030} y^3_{(n)} + a^y_{0040} y^4_{(n)} + \cdots \\
&+ \quad a^y_{0100} \theta_{(n)} + a^y_{0200} \theta^2_{(n)} + a^y_{0300} \theta^3_{(n)} + a^y_{0400} \theta^4_{(n)} + \cdots \\
&+ \quad a^y_{1000} x_{(n)} + a^y_{2000} x^2_{(n)} + a^y_{3000} x^3_{(n)} + a^y_{4000} x^4_{(n)} + \cdots \\
&+ \quad a^y_{1111} x_{(n)} \theta_{(n)} y_{(n)} \phi_{(n)} \,, \quad n = 1, \cdots N
\end{aligned} \tag{15}
$$

where N is the number of coincidence events considered in the analysis. The overdetermined set of equations (15) is a direct comparison of a reconstructed vertex position $y^{\text{Optics}}_{\text{Tg}}$ to the measured value $y^{\text{Measured}}_{\text{Tg}}$. Initially a consisten polynomial expansion to fourth-degree ($i + j + k + l \leq 4$) was considered, which depends on 70 different matrix elements a^y_{ijkl}. Using this ansatz in (12), χ^2-minimization function is written, serving as a input for simplex method. To be certain, that minimization will not stop in one of the potential local minima, robustness of the method was examined. This was done by checking the convergence of the minimization algorithm for a large number of randomly chosen initial sets of parameters (see Fig. 5). The result could be trusted, if (12) converges to same value for the majority of initial condidions. Small variations in χ^2 are allowed. They are caused by small matrix elements which are irrelevant for y_{Tg}, but are set so some non-zero value to additionally minimize χ^2 in a particular minimization process. These matrix elements could be easily identified and excluded when doing the robustness checks, because they are unstable and converge to a different value in each minimization process. In addition, Monte-Carlo simulation was considered for selection of the relevant matrix elements. In the end 25 least changing matrix elements were kept in the y_{Tg} matrix.

Next, SVD method was used to determine matrix elements for y_{Tg}. Linear set of equations (15) first needs to be re-written into an appropriate form (13):

$$
\begin{pmatrix}
1 & \phi_{(1)} & \cdots & x_{(1)}\theta_{(1)}y_{(1)}\phi_{(1)} \\
1 & \phi_{(2)} & \cdots & x_{(2)}\theta_{(2)}y_{(2)}\phi_{(2)} \\
1 & \phi_{(3)} & \cdots & x_{(3)}\theta_{(3)}y_{(3)}\phi_{(3)} \\
\vdots & \vdots & \ddots & \vdots \\
1 & \phi_{(N-2)} & \cdots & x_{(N-2)}\theta_{(N-2)}y_{(N-2)}\phi_{(N-2)} \\
1 & \phi_{(N-1)} & \cdots & x_{(N-1)}\theta_{(N-1)}y_{(N-1)}\phi_{(N-1)} \\
1 & \phi_{(N)} & \cdots & x_{(N)}\theta_{(N)}y_{(N)}\phi_{(N)}
\end{pmatrix}
\begin{pmatrix} a_{0000} \\ a_{0001} \\ \vdots \\ a_{1111} \end{pmatrix}
=
\begin{pmatrix} y_{\text{Tg}_{(1)}} \\ y_{\text{Tg}_{(2)}} \\ y_{\text{Tg}_{(3)}} \\ \vdots \\ y_{\text{Tg}_{(N-2)}} \\ y_{\text{Tg}_{(N-1)}} \\ y_{\text{Tg}_{(N)}} \end{pmatrix}, \tag{16}
$$

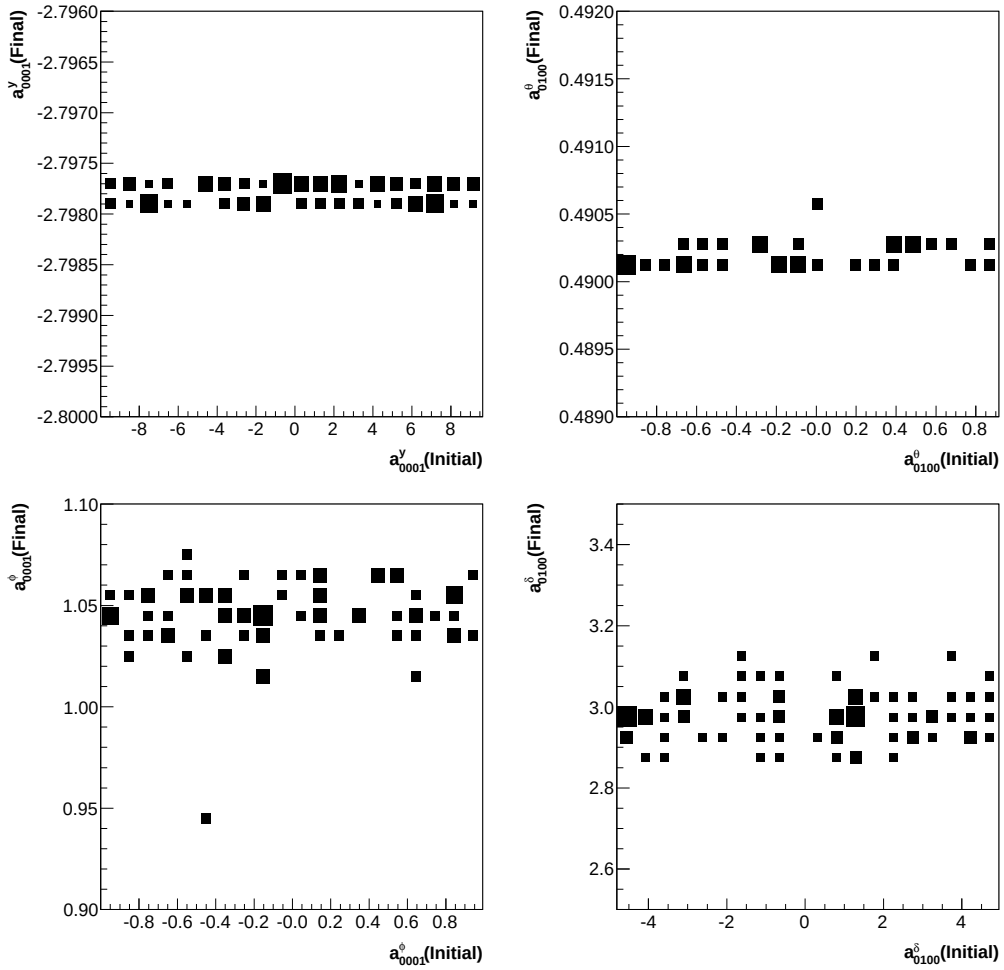

Figure 5: Robustness checks of simplex minimization method for chosen matrix elements $a^{\Omega_{Tg}}_{ijkl}$. The analysis was done for 100 initial randomly chosen conditions, for each target coordinate. The fact that the vast majority of the initial conditions converge to a single value, is an indication of the robustness of the method.

where vector $\mathbf{a}$ contains M unknown matrix elements, vector $\mathbf{b}$ contains N measured values of y_{Tg}, and matrix A is filled with the products of detector variables, that accompany matrix elements in the polynomial expansion (15) for each considered event. Once knowing matrix A, singular value decomposition was preformed and solution for a^{y}_{ijkl} found. The SVD analysis also began with thye initial 70 matrix elements. Since the solution, returned by this method, always represents the global minimum of χ^2-function,

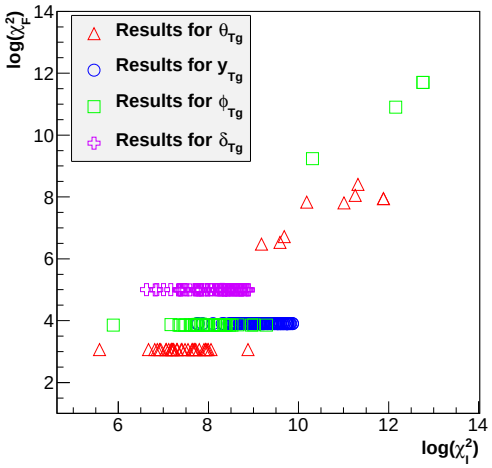

Figure 6: Values of the χ^2-function before and after simplex minimization for all four target coordinates. Method successfully converges to a single χ^2 value for wide range of initial conditions. Solution with smallest χ^2 represents the result used in the optics-matrix.

rubustness checks were not required. To extract the most relevant matrix elements, SVD method was not applied to one combined set of data (as in simplex method), but was used on each sets of experimental data seperately. From the comparison of the matrix-elements obtained with different calibration data, those that were changing less than 100 %, were selected. Matrix-elements that were changing more, should not be considered, since optics-matrix needs to be valid for all accumulated data. In the end 20 best matrix-elements were considered. With them analysis was done once more, to determine their final values. Calibration results are shown in figure 4. The values of most important elements are listed in table 1.

4.2.5. Angular coordinates

The relative optics calibration of the angular variables θ_{Tg} and ϕ_{Tg} was done with a use of sieve-slit data. With a use of sieve-slit collimator only particles going throught the holes could reach BigBite detectors. Others were stopped in 4 cm thick material of the slit. Particles coming from different holes could be well seperated and localized at the focal plane. Knowing the detector coordinates and the precise position of the corresponding hole in the sieve, target variables could be calculated. Considering reaction point at the

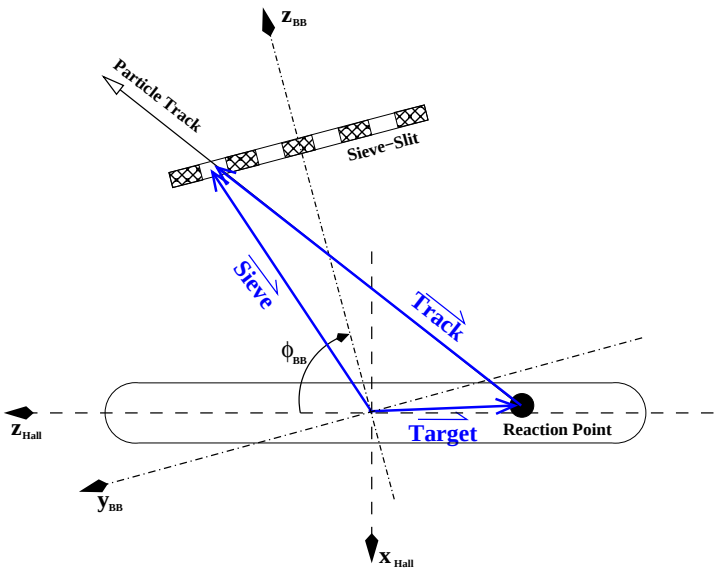

Figure 7: Layout of sieve-slit collimator relative to the target. Particle track going through a particular hole in the sieve is a difference between the position in the sieve-hole and position of the reaction-point. BigBite is positioned at $\Phi_{\rm BB} = -75^\circ$ with respect to the beam direction.

target (see Fig. 7), $\theta_{\rm Tg}$ and $\phi_{\rm Tg}$ can be expressed as

$$\tan\phi_{\rm Tg} = \frac{y_{\rm Sieve} - y_{Tg}}{z_{\rm Sieve} - z_{\rm Tg}}\,, \quad \tan\theta_{\rm Tg} = \frac{x_{\rm Sieve} - x_{\rm Tg}}{z_{\rm Sieve} - z_{\rm Tg}} \tag{17}$$

Knowing values of target variables, set of linear equations (7) can be written for considered events and matrix-elements determined using both numerical approcahes. For the calibration with the simplex method 30 matrix elements for $\theta_{\rm Tg}$ and 68 for $\phi_{\rm Tg}$ were considered. Robustness checks for both angular variables were made to ensure a global minima. The SVD analysis again started with 70 matrix-elements which were then reduced to 31 for $\theta_{\rm Tg}$ and to 39 for $\phi_{\rm Tg}$, considering only least changing matrix elements. Fig. 3 shows reconstructed sieve pattern. The majority of holes are reconstructed. Some are missing, because of specific geometric constraints during the calibration experiment that obscured them. Once sieve pattern was reconstructed, absolute calibration had to be preformed, to correct for any BigBite missalignment and misspointing. For that hyrdogen-elastic data were used. Comparing direction of q-vector from HRS-L with the calculated values $\theta_{\rm Tg}$ and $\phi_{\rm Tg}$, zero-order matrix elements could be properly determiend

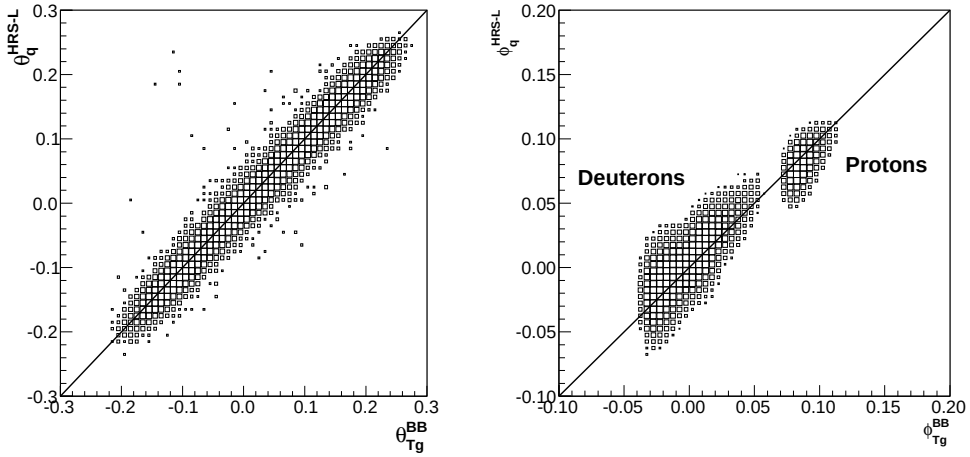

Figure 8: Calibration of in-plane and out-of-plane angles by comparing $\theta_{\rm Tg}$, $\phi_{\rm Tg}$ from HRS-L and BigBite.

and offsets corrected. In addition, precise distance between the target and collimator could be determiend, which could not be precisely measured due to physical obstacles during experiment. Sieve slit was positioned 1.13 m away from the target.

4.2.6. Momentum

The calibration of δ_{Tg} variable was done via comparison of the q-vector to the reconstructed BigBite momentum by using elastic scattering of electrons on hydrogen and deuterium. In the analysis $\delta_{\rm Tg}$ was considered only as a function of $x_{\rm Det}$ and $\theta_{\rm Det}$. Terms with y_{Det} and ϕ_{Det} could be neglected, since δ_{Tg} depends mostly on the out-of-plane variables. In addition, use of in-plane coodrinates in the analysis could result in bad matrix, due to strong ϕ_{Tg} dependence of elastic data. Considering only $x_{Det}\,, \theta_{Det}$ matrix elements δ_{Tg} can be expressed as

$$\frac{q_{\rm HRSL} - \Delta_{\rm Loss}}{p_{\rm Central}} - 1 = \delta_{\rm Tg} = a^{\delta}_{0000} + a^{\delta}_{1000} x_{Det} + a^{\delta}_{0100} \theta_{\rm Det} + \cdots . \tag{18}$$

In order to obtain an optics-matrix, that is valid for all kinds of particles (protons and deuterons), energy-losses Δ_{Loss} for particle transport through target enclosure and BigBite had to be well known and under control. For the estimation of losses Bethe-Bloch formula [10] was considered. Since energy-losses were significant Bethe-Bloch formula

had to be integrated over complete particle track, for each type of particles and each initial momentum. Resulting corrections that were considered in (18) are shown in figure 9.

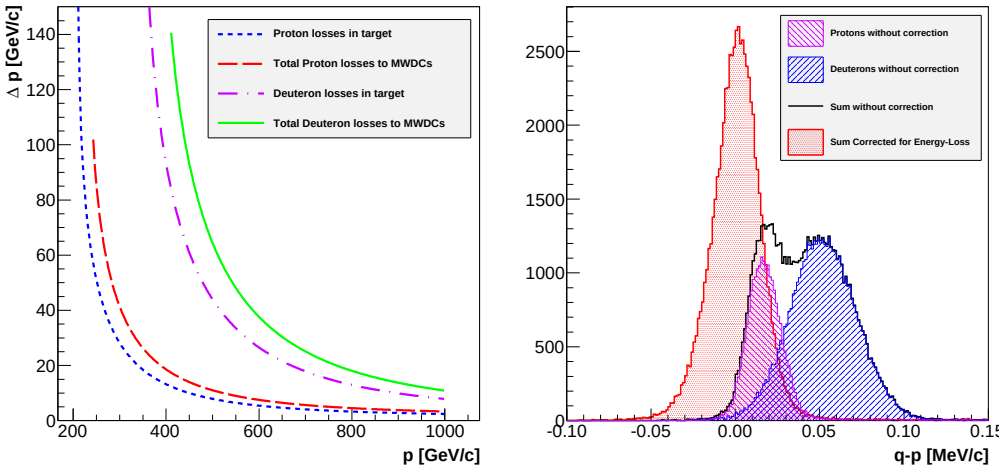

Figure 9: [Left] Proton and deuteron momentum losses inside the target and the total momentum losses to the MWDCs. [Right] The momentum resolution is increased significatnly with proper consideration of momentum losses.

Elastic data, available for calibration, covered only half of the BigBite momentum acceptance. They include data between 450 MeV/c and 700 MeV/c. To calibrate low-momentum region from 200 MeV/c to 450 MeV/c additional calibration data were required. For that quasi-elastic ^{3}He data were considered using the infomration from the dE- and E-planes. Knowing the scintillator properties, the energy-deposit in each plane could be directly connected to a particle momentum. In particular we were interested in the particle momentum at the well defined point, where particles have just enough energy to exit the scintillators. This is known as a punch-through point. Beside punch-through points two other points with exactly known energy-deposit in dE- and E-planes were considered (see Fig. 10). With the momentum information from these points, complete momentum calibration was possible. For the determination of δ_{Tg} matrix elements both numerical approaches were again considered. Due to limitations with available data, search for most stable matrix-elements with the SVD method was not performed. A complete expansion to fifth-order was considered in both techiques. However, since

only two-variable dependence was considered this represents 21 different matrix elements. Comparison of the most relevant matrix elements for both numerical approaches is show in table 1. Fig. 10 also shows that δ_{Tg} matrix is well-behaved, since the reconstructed momentum agrees with the simulation for the complete momentum acceptance of BigBite for both protons and deuterons.

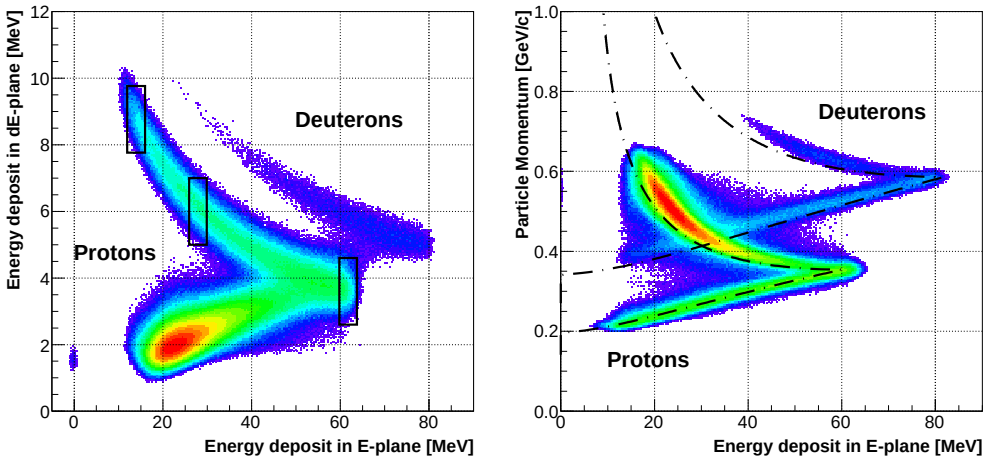

Figure 10: [Left] Energy-losses in a thin 3 mm dE-plane vs. energy-losses in a thicker 3 cm E-plane. Punch-through points, where protons and deuterons have just enough energy to penetrate through both scintillation planes are clearly visible. Black boxes show sections of events with precisely determined momentum, that were used in the δ_{Tg} calibration. [Right] Energy-losses in E-plane scintillator as a function of particle momentum for ^{3}He data. Deuterons can be clearly distinguished from protons. Measurements agree well with the simulation, shown with dashing line.

4.2.7. Resolution of the results

The quality of the BigBite optics was also studied. The resolution of vertex-position was estimated from the difference between reconstructed y_{Tg} and the true position at the target, by taking the width (sigma) of the obtained distribution. The analysis was done using 1 GeV and 2 GeV quasi-elastic carbon data. Fig. 11 shows resolution as a function of particle momentum. The width of the peak decreases with the increasing momentum, reaching the best resolution $\sigma_{Tg_y} = 1.0\,\mathrm{cm}$ at $p = 0.55\,\mathrm{GeV/c}$. The worsening of the resulution at momenta $p \geq 0.6\,\mathrm{GeV/c}$ is caused by the errors in the optics matrix. Due

to small amount of available data for high momenta, matrix could not be precisely calibrated for that momentum reagion.

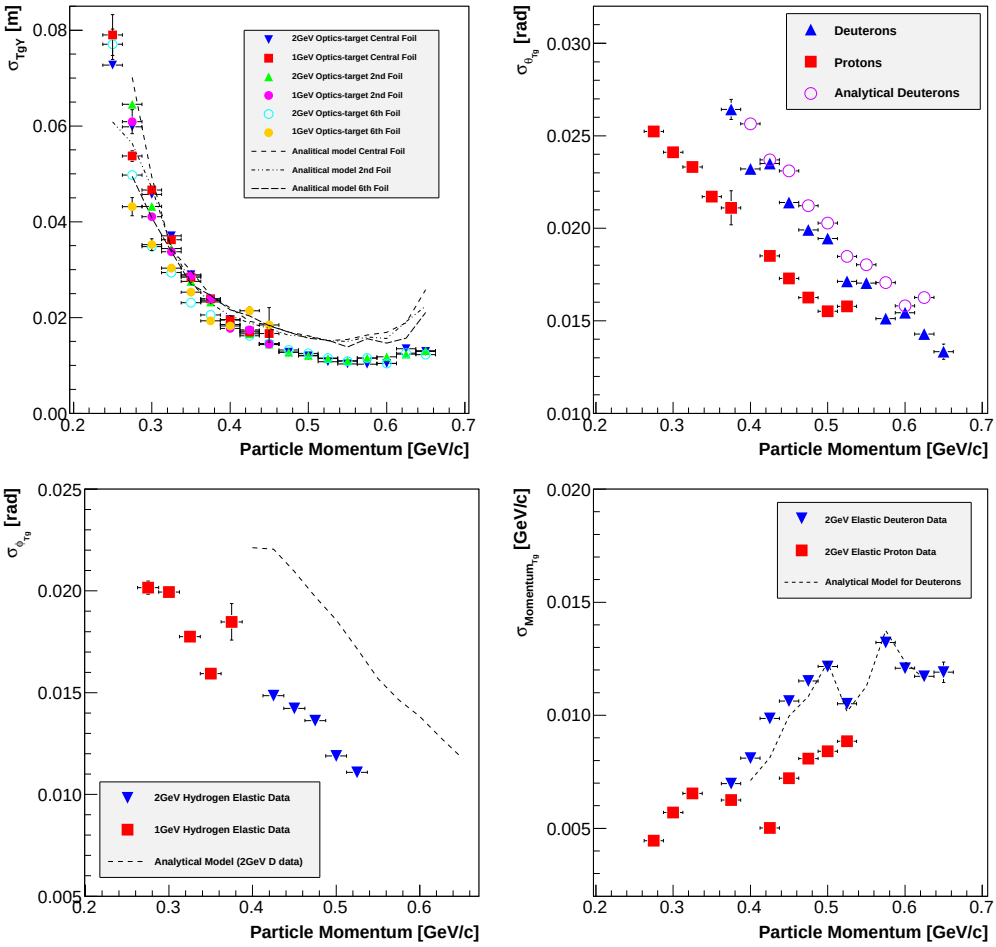

Figure 11: Resolution of y_{Tg}, θ_{Tg}, ϕ_{Tg} and δ_{Tg} as a function of particle momentu, detected in BigBite.

Resolution of the θ_{Tg} and ϕ_{Tg} was estimated from their comparison to the corresponding angles determined from the momentum-transfer vector $\vec{q}$, using elastic hydrogen and deuterium data. The direction of $\vec{q}$ is calculated from the HRS-L data. The resolution

of calculated $\theta^{\vec{q}}_{Tg}$ and $\phi^{\vec{q}}_{Tg}$ follow relations

$$d\theta^{\vec{q}}_{Tg} \approx \csc\Phi_{\rm HRS} d\theta_{\rm HRS}, \quad d\phi^{\vec{q}}_{Tg} \approx \csc\Phi_{\rm HRS}\left[\csc\Phi_{\rm HRS} - \frac{E_{\rm Beam}}{E_{\rm HRS}}\right] d\phi_{\rm HRS}\,, \tag{19}$$

where $E_{\rm HRS}$ is the central momentum of the HRS-L spectrometer and $\Phi_{\rm HRS}$ its central scattering angle. With the nominal resolution of HRS-L spectrometer [3] is the resolution of q-vector direction estimated to (≥ 5 mrad) for the vertical angle and to (≥ 0.43 mrad) for the horizontal angle. This contributions were subtracted in squares from calculated peak widths to get final BigBite resolution. Results are shown in Fig. 11 as a function of particle momentum. Resolution strong momentum dependence is caused by the multiple-scattering [**?**], happening inside the spectrometer and the target. Multiple-scattering also explains different resolution for protons and deuterons, since peak broadening stronly depends on the particle mass. Biggest contribution comes from air inside BigBite and target cell-wall. It is estimated to 7 mrad (sigma) for 550 MeV/c protons and to 13 mrad for 550 MeV/c deuterons.

The resolution of δ_{Tg}....

5. Summary

6. Acknowledgments

This work was supported in part by the U.S. Department of Energy and the U.S. National Science Foundation. It is supported by DOE contract DE-AC05-06OR23177, under which Jefferson Science Associates, LLC, operates the Thomas Jefferson National Accelerator Facility.

References

[1] D.J.J. Lange *et. al.*, Nucl. Instr. and Meth. **A 406** (1998) 182.

[2] D.J.J. Lange *et. al.*, Nucl. Instr. and Meth. **A 412** (1998) 254.

[3] J. Alcorn *et. al.*, Nucl. Instr. and Meth. **A 522** (2004) 294.

[4] R. Lindgren, B. E. Norum, J. R. M. Annand, V. Nelyubin (spokespersons), *Precision measurements of electroproduction of* $\pi 0$ *near threshold: a test of chiral QCD dynamics*, TJNAF Experiment E04-007.

[5] J.-P. Chen, E. Cisbani, H. Gao, X. Jiang, J.-C. Peng (spokespersons), *Measurement of single target-spin asymmetry in semi-inclusive* n $\uparrow$ $(\mathrm{e},\mathrm{e}'\pi^-)$ *reaction on a transversely polarized* ^{3}He *target*, TJNAF Experiment E06-010.

[6] E. Cisbani, H. Gao, X. Jiang, (spokespersons), *Target single spin asymmetry in semi-inclusive deep-inelastic* $(\mathrm{e},\mathrm{e}'\pi^+)$ *reaction on a transversely polarized* ^{3}He *target*, TJNAF Experiment E06-011.

[7] S. Choi, X. Jiang, Z.-E. Meziani, B. Sawatzky, *Precision measurements of the neutron d_2: towards the electric χ_E and magnetic χ_B color polarizabilities*, TJNAF Experiment E06-014.

[8] S. Širca, S. Gilad, D. W. Higinbotham, W. Korsch, B. E. Norum, *Measurement of A_x and A_z asymmetries in the quasi-elastic* $^3\vec{\mathrm{He}}\,(\vec{e},e'd)$, TJNAF Experiment E05-102.

[9] W.H. Press , Numerical Recipes in C, *Second Edition*, Cambridge University Press, Cambridge, 1992.

[10] W.R. Leo, Techniques for Nuclear and Particle Physics Experiments, Springer-Verlag, Heidelberg, 1987.

[11] J.C. Lagarias *et. al.*, SIAM J. Optim. 9 (1998) 112

[12] K.I.M. McKinnon, SIAM J. Optim. 9 (1998) 148.

.